Flinders UNIVERSITY

Quantitative evaluation of facet deflection, stiffness, strain and failure load during simulated cervical spine trauma

Ryan D. Quarrington, John J Costi, Brian J.C. Freeman, Claire F. Jones

PII: S0021-9290(18)30149-0
DOI: https://doi.org/10.1016/j.jbiomech.2018.02.036
Reference: BM 8598

To appear in: *Journal of Biomechanics*

Accepted Date: 28 February 2018

Please cite this article as: R.D. Quarrington, J.J. Costi, B.J.C. Freeman, C.F. Jones, Quantitative evaluation of facet deflection, stiffness, strain and failure load during simulated cervical spine trauma, *Journal of Biomechanics* (2018), doi: https://doi.org/10.1016/j.jbiomech.2018.02.036

TITLE: Quantitative evaluation of facet deflection, stiffness, strain and failure load during simulated cervical spine trauma

KEY WORDS: Cervical facet dislocation; Biomechanics; Facet fracture; Shear; Flexion

WORD COUNT: 3780 words

MANUSCRIPT TYPE: Original Article

AUTHORS:

Ryan D Quarrington, B. Eng (Mechanical and Sports) - Corresponding Author

School of Mechanical Engineering, The University of Adelaide

Centre for Orthopaedic & Trauma Research, Adelaide Medical School, The University of Adelaide

Spinal Research Group

Address: Level 7, Adelaide Health and Medical Sciences Building, North Terrace, Adelaide, SA, 5000

Email: ryan.quarrington@adelaide.edu.au

Phone: +61882223106

John J Costi, PhD

Biomechanics and Implants Research Group, The Medical Device Research Institute, College of Science and Engineering, Flinders University

Address: GPO Box 2100, Adelaide, South Australia 5001, Australia

Email: john.costi@flinders.edu.au

Phone: +61882013323

Brian J C Freeman, MB, BCh, BAO, FRCS (Tr & Orth), FRACS (Ortho), DM

The Spinal Injuries Unit, Royal Adelaide Hospital, Adelaide, South Australia

Centre for Orthopaedic & Trauma Research, Adelaide Medical School, The University of Adelaide

Address: Spinal Injuries Unit, Level 5G, Royal Adelaide Hospital, Port Road Adelaide, SA 5000, Australia

Email: brian.freeman@sa.gov.au

Phone: +61429120991

Claire F Jones, PhD

Centre for Orthopaedic & Trauma Research, Adelaide Medical School, The University of Adelaide

Spinal Research Group

School of Mechanical Engineering, The University of Adelaide.

Address: Level 7, Adelaide Health and Medical Sciences Building, North Terrace, Adelaide, SA, 5000

Email: claire.jones@adelaide.edu.au

Phone: +61883132850

ABSTRACT

Traumatic cervical facet dislocation (CFD) is often associated with devastating spinal cord injury. Facet fractures commonly occur during CFD, yet quantitative measures of facet deflection, strain, stiffness and failure load have not been reported. The aim of this study was to determine the mechanical response of the subaxial cervical facets when loaded in directions thought to be associated with traumatic bilateral CFD – anterior shear and flexion. Thirty-one functional spinal units (6×C2/3, C3/4, C4/5, and C6/7, 7×C5/6) were dissected from fourteen human cadaver cervical spines (mean donor age 69 years, range 48-92; eight male). Loading was applied to the inferior facets of the inferior vertebra to simulate the *in-vivo* inter-facet loading experienced during supraphysiologic anterior shear and flexion motion. Specimens were subjected to three cycles of sub-failure loading (10 to 100 N, 1 mm/s) in each direction, before being failed in a randomly assigned direction (10 mm/s). Facet deflection, surface strains, stiffness, and failure load were measured. Linear mixed-effects models (α=0.05; random effect of cadaver) accounted for variations in specimen geometry and bone density. Specimen-specific parameters were significantly associated with most outcome measures. Facet stiffness and failure load were significantly greater in the simulated flexion loading direction, and deflection and surface strains were higher in anterior shear at the non-destructive analysis point (47 N applied load). The sub-failure strains and stiffness responses differed between the upper and lower subaxial cervical regions. Failure occurred through the facet tip during anterior shear loading, while failure through the pedicles was most common in flexion.

KEY WORDS: Cervical facet dislocation; Biomechanics; Facet fracture; Shear; Flexion

INTRODUCTION

Traumatic cervical facet dislocation (CFD) is often associated with devastating spinal cord injury, resulting in tetraplegia in up to 87% of cases (Hadley et al., 1992; Payer and Schmidt, 2005). CFD may be unilateral or bilateral, with bilateral facet dislocation (BFD) more often resulting in complete spinal cord injury (Allen et al., 1982; Quarrington et al., 2017). These injuries occur most commonly, and are most often survived, in the sub-axial region (C3-T1). They are frequently a result of traffic and sporting accidents, and falls (Allen et al., 1982; Quarrington et al., 2017), during which the external loading applied to the neck can be complex and variable.

BFD is thought to result from a *global, supra-physiologic* flexion moment about the subaxial cervical spine, caused by axial compressive forces applied to the head with large anterior eccentricity (Allen et al., 1982; Cusick and Yoganandan, 2002; Huelke and Nusholtz, 1986; White and Panjabi, 1990), or from inertial motion of the head during high deceleration events (Huelke and Nusholtz, 1986). In head-first impact tests of head-neck specimens, BFDs occurring in the lower cervical spine have been associated with local intervertebral flexion and anterior shear motions (Hodgson and Thomas, 1980; Ivancic, 2012; Nightingale et al., 2016). The inertial injury mechanism of BFD was validated in one experimental series (Ivancic et al., 2007, 2008; Panjabi et al., 2007) in which incrementally increasing, sagittal decelerations were applied to cervical motion segments (with a head mass surrogate) until dislocation occurred. Large flexion angles and anterior shear displacements were the dominant sagittal *intervertebral* motions observed during the injury event (Panjabi et al., 2007). Interestingly, no cervical facet fracture-dislocations have been produced experimentally, yet facet fractures are associated with up to 88% of clinical CFD cases (Foster et al., 2012). It has been suggested that concomitant fracture may be due to a large

component of anterior shear in the local injury vector (Foster et al., 2012), but this has not been validated experimentally.

Studies that investigated the kinematics of cervical vertebrae during dynamic spinal motion have assumed that the anterior and posterior anatomy act as a rigid body (Ivancic et al., 2007, 2008; Panjabi et al., 2007). However, the high incidence of facet fracture associated with CFD would suggest that large loads are transmitted through this joint during the injurious motions, and one could expect substantial bending of the facets to occur prior to mechanical failure. In addition, sagittal bending of the facets in excess of 14°, relative to the vertebral body, was observed in a *lumbar* specimen during replicated *physiological* intervertebral flexion (Green et al., 1994). The magnitude of facet deflection and the mechanical response of the sub-axial cervical facets during loading to simulate supra-physiologic anterior shear and flexion motions have not been reported.

The mechanical response of the cervical facet capsule during simulated trauma has been well characterized, particularly regarding soft-tissue strains during 'whiplash' events (Cholewicki et al., 1997; Panjabi et al., 1998; Siegmund et al., 2008; Siegmund et al., 2001); however, strain data is not available for the bony facet. Investigations of the load-bearing capacity (Hakim and King, 1976; King et al., 1975; Pollintine et al., 2004), failure mechanisms (Cyron et al., 1976), fatigue strength (Cyron and Hutton, 1978) and surface strain response (Schulitz and Niethard, 1980; Shah et al., 1978; Suezawa et al., 1980) of the *lumbar* facets and neural arch have been performed, but similar analyses have not been reported for the subaxial cervical spine, or during simulated facet dislocation. Quantitative measures of the mechanical response of the cervical facets to simulated traumatic loading may be important for validation

of computational models of cervical trauma and to inform design of advanced anthropometric test device (ATD) necks and associated injury criteria.

The aim of this study was to quantify the sagittal deflection, apparent stiffness, surface strain and failure load of subaxial cervical inferior facets under loads simulating the proposed injury vectors of supraphysiologic *in-vivo* flexion and anterior shear motions.

METHODS

Specimen preparation

Thirty-one functional spinal units (FSUs); six C2/3, six C3/4, six C4/5, seven C5/C6 and six C6/C7, were dissected from fourteen fresh-frozen human cadaver cervical spines (mean donor age 69 years, range 48-92; eight male). Radiographs and high-resolution computed tomography (CT) scans (Toshiba Aquilion ONE, Otawara, Japan; 0.5 mm slice thickness, 0.3 mm in-plane resolution) were obtained and each specimen was screened for excessive degeneration, injury and disease by a senior spinal surgeon. Average volumetric bone mineral density (vBMD) was quantified from CT using a calibration phantom (Mindways Software Inc., Texas, USA) and 'FIJI' image analysis software (1.51p, ImageJ, Maryland, USA) (Schindelin et al., 2012) (Figure S1a). Vertebral endplate depths and sagittal facet angles were measured using FIJI (Figure S1b and S1c).

Specimen musculature was removed and the vertebral disc and bilateral facet joint capsules were preserved (Figure 1a). The vertebral bodies of each FSU were embedded in polymethylmethacrylate (PMMA; Vertex Dental, Utrecht, Netherlands) using a custom adjustable mold (Figure 1b). To assist with fixation a wood screw was inserted through the vertebral bodies and disc, and steel wire was wrapped around the vertebral bodies and

through the transverse foramen (Figure 1a); excess wire and the screw-tip protruded from the superior endplate of the superior vertebra into a rectangular embedding cavity approximately 50 mm in length. The FSU was placed in the mold which was then filled with PMMA. A support bar was positioned within the spinal canal along the posterior surfaces of the vertebral bodies and was fixed to the PMMA block (Figure 1b and c). Three types of support bars, accommodating variation in specimen geometry, were used to prevent embedding failure: 1) 90x20x1.5 mm aluminum; 2) 90x20x5 mm steel; and, 3) 90x10x5 mm steel.

Mechanical loading

Each specimen-PMMA assembly was rigidly mounted to the base of a biaxial materials testing machine (8874, Instron, High Wycombe, UK) via a custom support apparatus attached to a rotary table (VU150, Vertex, Taichung City, Taiwan) (Figure 2). Using the rotary table, the inferior articular facet surfaces of the inferior vertebrae were positioned relative to the actuator to simulate the loading vectors thought to be applied by the opposing facets during *in-vivo*, supraphysiologic flexion and anterior shear motions (Figure 2). A 10 N pre-load and then three cycles of sub-failure loading to 100 N (a non-destructive load determined from pilot testing) were applied bilaterally to the geometric center of each articular facet surface at 1 mm/s using 6 mm diameter hemispherical loading pins, in each loading direction. The simulated 'flexion' load was directed perpendicular to the facet surfaces to represent the inter-facet forces experienced during *local*, *non-physiologic* compressive-flexion motion, while the 'anterior-shear' load was directed parallel to the inferior vertebral endplate (Figure 2). The posterior elements of the superior vertebra provided a physiological boundary condition for the loaded inferior facets. Uniaxial strain gauges (FLA-1-23-1L, TML, Tokyo, Japan) were attached to the loading pins to ensure that symmetrical loading was applied to the bilateral facets during each test. Following completion of the sub-failure testing, each

specimen was loaded to failure in one of the two directions (randomly assigned) at 10 mm/s. The non-destructive and destructive loading rates chosen were the maximum possible to obtain sufficient motion-capture data.

Instrumentation and data collection

The inferior vertebra of each specimen was instrumented to measure the mechanical response of the bilateral inferior facets to loading. Tri-axial rosette strain gauges (FRA-1-23-1L, TML, Tokyo, Japan) and custom light-weight motion capture marker-carriers (Optotrak Certus, Northern Digital Inc., Ontario, Canada) were fixed to the bilateral inferior facet bases and tips, respectively (Figure 3). A third marker-carrier was attached to the inferior vertebral body via a K-wire (Figure 3). Anatomical landmarks were digitised using a 1 mm diameter spherical probe tip (Figure S2).

Loads and actuator position were measured by a biaxial load cell (Dynacell ±25 kN, Instron, High Wycombe, UK) and an internal linear variable differential transducer (LVDT), respectively (Figure 2). A six-axis load cell (MC3A-6-1000 ±4.4 kN, AMTI, Massachusetts, USA) was connected in series to measure off-axis loads and moments. Failure tests were recorded at 100 Hz using a high-speed camera (i-Speed TR, Olympus Corporation, Tokyo, Japan).

Data processing

Data were processed using custom MATLAB code (R2015a, Mathworks, Massachusetts, USA). Strain gauge, LVDT, load cell, and motion capture data were filtered using a second-order, two-way Butterworth low-pass filter. A cut-off frequency of 100 Hz was used for all except the motion capture data (30 Hz).

The aforementioned 4.4 kN six-axis load cell was used to monitor the 10 N pre-load, and the 25 kN biaxial load cell controlled the 100 N load-limit for each test; however, a substantial 'shear' load (perpendicular to the direction of the applied load) occurred during the simulated anterior-shear tests, due to the inclined angle of the facets in this specimen orientation. This off-axis load appeared to cause mechanical cross-talk in the biaxial load cell, as 100 N of applied load (through the axis of the loading pins) was not consistently measured by the six-axis load cell during anterior-shear tests. Therefore, to ensure the outcome measures for each specimen were obtained at an equivalent load, values corresponding to an applied load of 47 N (the highest load reached by all specimens) as measured by the six-axis load cell, were determined. This load is comparable to physiological cervical facet joint forces (Jaumard et al., 2011; Kumaresan et al., 2001).

Load-displacement plots were generated for the sub-failure tests, and apparent facet stiffness (N/mm) was determined from the slope of the linear region (Figure 4). Maximum principal and shear strains were calculated from the output of each rosette gauge. Local anatomical coordinate systems, consistent with International Society of Biomechanics' recommendations for spinal joints (Wu et al., 2002), were defined for the vertebral body and facets using the anatomical landmark coordinates illustrated in Figure S2. Angular deflection of the facets relative to the vertebral body (in degrees) was calculated by solving for Euler angles using a *z*-*y*-*x* sequence (Robertson, 2004); facet deflections were only appreciable in the sagittal plane (about *z*). For the destructive tests, the instant of initial failure (of either one or both facets, defined as a distinct reduction in load and confirmed using high-speed camera footage) was identified (Figure 4), and the applied load, facet deflection and surface strains

were determined at this point. The failure mode of each specimen was determined from viewing the high-speed camera footage and by visual inspection of the specimen.

Data from the last cycle of each non-destructive test were used for statistical analyses. Where anatomical asymmetry led to loading asymmetry, the larger of the two strain and deflection values were used.

Statistics

Statistical analyses were performed using SPSS v22 (IBM, Illinois, USA). Eight linear mixed-effects models (LMM) were developed to identify if loading direction was significantly associated with the following outcome measures: non-destructive 1) facet stiffness, 2) maximum principal strain, 3) maximum shear strain and 4) sagittal deflection; and, 5) applied load, 6) maximum principal strain, 7) maximum shear strain, and 8) sagittal deflection at failure. Each model was developed as follows. Firstly, Shapiro-Wilk and Levene tests were performed to assess normality and homogeneity of variance of the dependent variables, respectively. If required, statistically significant outliers were removed and/or data was log-transformed to meet these criteria. The effect of test direction was assessed in all models, and this effect was adjusted for spinal level, the interaction of spinal level with test direction, donor demographics, specimen bone quality and geometry, and the type of support bar. As multiple specimens from the same donor were used in this study, a random effect of spinal level, nested within cadaver ID, was included. Each model was refined using a manual backward step-wise approach until only significant predictors remained (α=0.05).

RESULTS

Donor and specimen details, and failure outcomes, are provided in Table 1. One C3/4 specimen (Test #1) was omitted from all analyses due to technical difficulties during testing. Failure data was not available for a further six specimens due to: inadequate fixation of the specimen in the embedding material (N=2; #13 and #16); poor bone quality resulting in loading pins puncturing the facets or fracture occurring at the bone-screw interface (N=3; #2, #12 and #17); and, slipping of the rotary table (N=1; #4).

The eight final multivariable LMMs are presented in Tables S1 and S2 in supplementary material. A significant interaction between test direction and specimen level was associated with apparent facet stiffness ($p=0.007$), when adjusted for vBMD and support bar type (Table S1.1). Post-hoc analysis demonstrated that specimens were significantly stiffer when loaded in the flexion direction compared to the anterior shear direction for all spinal levels (Figure 5, Table S3 in supplementary material), but this difference was less pronounced in the lower levels (C6 and C7) compared to the upper levels (C3-C5). In the anterior shear loading direction, stiffness was significantly higher for C6 and C7 vertebrae compared to C5 (Table S4: C5 vs C6, $p=0.006$; C5 vs C7, $p=0.010$), while the inverse relationship tended towards significance for the flexion loading direction (Table S4: C5 vs C6, $p=0.152$; C5 vs C7, $p=0.099$) (Figure 5).

Lower stiffness measurements for the anterior shear loading direction corresponded with significantly larger maximum principal strains ($p<0.001$), shear strains ($p<0.001$), and sagittal facet deflections ($p=0.009$) compared to specimens loaded under simulated flexion, when adjusted for gender and vertebral body depth, gender, and vBMD, respectively (Figure 6, Table S1.2-S1.4).

Failure load was significantly higher in simulated flexion than for specimens failed in anterior shear (p=0.001), when adjusted for vBMD and support bar type (Figure 7, Table S2.1). Sagittal facet deflection at initial failure was also larger in flexion (p=0.001). The highest failure load was 1.2 kN, and deflections ranged from 1.15° to 5.58° (mean = 2.60±0.34°) for anterior shear and from 2.55° to 10.24° (mean = 5.75±0.73°) for flexion. There was no statistical difference between the maximum principal (p=0.566) and shear strains (p=0.164) observed at failure for the two loading directions (Figure 7, Tables S2.2 and S2.3). Principal and shear strains ranged from 815 to 7,394 microstrain (με) and 2,676 to 16,897 με for anterior shear, and from 852 to 5,858 με and 739 to 8,545 με for the flexion loading direction, respectively.

Two distinct fracture locations were identified (Figure 8). All specimens that were loaded destructively in the anterior shear direction failed through the inferior facet tips (13/13 specimens; Table 1). Of the eleven specimens tested to failure under simulated flexion, six fractured through the pedicles, three through the facet bases, and two through the facet tips (Table 1).

DISCUSSION

Despite the potentially devastating consequences of CFD, little published data exists regarding the biomechanics underlying this injury mechanism. The mechanical response of the subaxial facets, which are often fractured during CFD (Allen et al., 1982; Foster et al., 2012), have not previously been investigated. In this present study, bilateral loading was applied to the inferior facets of subaxial cervical vertebrae in directions that replicate traumatic anterior shear and flexion; these motions are thought to be associated with CFD

(Allen et al., 1982; Cusick and Yoganandan, 2002; Hodgson and Thomas, 1980; Ivancic, 2012; Nightingale et al., 2016; White and Panjabi, 1990). Facet stiffness was higher in flexion, which corresponded to higher sagittal deflections and sub-failure surface strains when compared to the anterior shear loading direction. The strain and stiffness responses differed between the upper and lower cervical regions. Failure load was higher in flexion, and distinct failure locations were observed for the two loading directions in most cases.

There is little published data regarding cervical facet biomechanics with which to compare our results. Wang *et al*. (2012) measured average C3 and C4 inferior facet uniaxial strains of 42 and 38 microstrain (με), respectively, at 20° of flexion applied to a four-vertebrae FSU; they did not apply anterior shear. These values are lower than, but comparable to, the maximum principal strains measured during non-destructive flexion testing in the present study (69±8 με, Figure 6a).

Maximum principal and shear strains were both significantly larger (at 47 N of applied load) during non-destructive simulated anterior shear motion than for simulated flexion motion (Figure 6). The strain response and apparent stiffness of the facets were significantly different in the upper and lower regions of the subaxial cervical spine. Maximum shear strains were significantly higher at the lower spinal levels than at C3 and C4, for both loading directions ($p=0.001$, Table S1.3). Interestingly, no significant differences in strains were observed at failure between loading directions or between spinal levels (Figure 7, Tables S2.3 and S2.4). This was unexpected, given that the failure locations were distinctly different between loading direction groups; however, strain measurements of bone are highly dependent on the anatomical location of the gauge, which was remote to the fracture sites. A difference in

strain response may have been observed if gauges were positioned on the pedicles and facet tips.

Apparent facet stiffness was significantly higher in the simulated flexion loading direction than anterior shear at all spinal levels, but this difference was less pronounced for the C6 and C7 vertebrae (Figure 5, Table S3). We hypothesize that this is due to the change in facet and pedicle orientation observed at the lower cervical levels (Panjabi et al., 1991; Panjabi et al., 1993), although facet angle was not a significant predictor in the final multivariable model. 'Facet stiffness' is a difficult parameter to interpret as the axis about which the facet deflects will be different for the two tested orientations. This will alter the contributions from the other posterior elements in resisting the applied loads – the term 'apparent facet stiffness' was used to reflect this. It is likely that larger stiffness values observed in the flexion testing orientation are, in part, due to increased contributions from the pars interarticularis and the pedicles.

Sagittal angular deflections of the cervical facets (relative to the vertebral body) at the time of failure were significantly larger in flexion than for anterior shear loading (Figure 7), with one specimen demonstrating facet deflection in excess of 10°. Our results indicate that the vertebral body and posterior elements are unlikely to be well represented as a single rigid body during simulated cervical trauma. This should be considered during kinematic analyses of motion segment injury involving the posterior elements by modelling the anterior and posterior anatomy of each vertebrae as separate rigid bodies and measuring their motions independently.

The mechanism of failure was generally different for the two simulated loading modes, and this difference was associated with significantly different failure loads (Figure 7). Bending of the facets during simulated anterior shear loading caused the point of load application to translate inferiorly towards the facet tip. We hypothesize that this may be representative of the change in facet articulation contact during *in-vivo* anterior shear motion (Figure 9). As this translation occurred, the volume of bone beneath the loading pin decreased until fracture occurred through the facet tip (13/13 specimens) (Figure 9). This fracture location is consistent with that described in radiographic reports of CFD (Allen et al., 1982). In contrast, for most specimens (6/11) that were failed in the simulated flexion orientation, the point of contact of the loading pin remained constant, and failure occurred through the pedicles or the facet base (Figure 9, Table 1). In the two specimens that fractured through the facet tip in the flexion loading direction, substantial translation of the loading pin was observed (similar to that observed for the anterior-shear loading mode), and the corresponding failure loads were lower than the other flexion specimens. The failure loads for pedicle fractures observed in the present study were considerably lower than those recorded for the lumbar spine (Cyron et al., 1976), likely due to the smaller size of the cervical vertebrae. No similar data exists for the cervical posterior elements, or for facet tip fractures. Facet tip, and facet base and pedicle fractures are commonly observed clinically, and correspond to AOSpine subaxial cervical spine facet injury classifications F2 and F3, respectively (Vaccaro et al., 2016).

The information presented in the current study may assist with developing improved computational models of cervical spinal motion and trauma. The non-destructive results suggest that the stiffness and strain responses of the posterior elements in the upper and lower subaxial regions should be considered independently when modelling the cervical spine. For example, the final multivariable LMM (Table S1.2) indicates that maximum principal strains

observed at the C6 and C7 facet bases during sub-failure loading will be significantly larger than those experienced in the upper cervical spine. Gender, vertebral size, or vBMD were significant variables in six of the eight LMMs (Tables S1 and S2), indicating that these specimen-specific parameters are important to consider when developing and validating computational models concerned with the cervical facets.

Substantial off-axis shear loads were observed during the anterior shear tests, due to the inclined angle of the facets in this specimen orientation. We chose to define outcome measures for each loading direction at an equivalent applied load (disregarding the off-axis loads), as this may be most useful for validation of computational models; however, the presence of these shear loads may be important to describe the dynamic facet loads experienced during cervical trauma. The off-axis loads recorded at the non-destructive analysis time-point, and at the point of initial failure, are reported in Table S5 in supplementary material. Additionally, the non-destructive analysis was repeated using outcome measures determined at an equivalent resultant sagittal load ($\sqrt{[\text{axial load}^2 + \text{shear load}^2]}$) of 60 N (the highest resultant load reached by all specimens). The results of this analysis were the same for all outcome measures except maximum principal strain, in which the test direction*spinal level interaction was significant (Tables S6 and S7 in supplementary material).

Physiological boundary conditions are an important consideration of biomechanical testing. 'Support bar type' was significant in 50% of the final LMMs and was associated with three of the four destructive outcome measures (Tables S1 and S2), demonstrating that minor variations in boundary conditions significantly influenced the measured facet response. This ex-vivo model included the superior adjacent vertebra to provide a boundary condition for the

loaded posterior elements. Pilot testing demonstrated that facets were stiffer, and deflections were smaller, when the superior adjacent facets were present, rather than resected. However, we did not apply a boundary condition to the inferior vertebral endplate to replicate the opposing vertebral body at the level of injury. We believe that such a boundary condition may influence the failure mechanisms, as the vertebral body and intervertebral disc may restrict large flexion motions (Allen et al., 1982).

To permit the same loading method for both test directions, hemispherical loading pins were used to apply quasi-static point loads to the facets; however, this may not be not representative of *in-vivo* facet loading conditions. Point loading may have induced higher stresses at the point of application leading to the 'punctured' facets that occurred in three specimens (these specimens were excluded from failure analysis), although two of these specimens also had the lowest vBMD values. The quasi-static loading rates applied in this study are lower than the 3 m/s thought necessary to cause cervical injury due to head-impact loading (McElhaney et al., 1979; Nightingale et al., 1996; Van Toen et al., 2014); however, these rates permitted accurate control of the test machine during non-destructive testing, and ensured that sufficient motion capture data was acquired during the failure tests. Importantly, clinically relevant fractures were observed for most specimens.

This study provides information about the mechanical response of the subaxial cervical inferior facets when loaded in directions that simulate the injury mechanisms of bilateral facet dislocation. When loaded in flexion, apparent stiffness and failure load of the cervical facets were greater, which corresponded to larger sagittal angular deflections and higher sub-failure surface strains when compared to the anterior shear loading direction. The stiffness and strain responses differed between the upper and lower subaxial cervical regions, and most

outcome measures were significantly associated with donor gender, specimen size or bone quality. Facet fractures occurred in all specimens that were loaded to failure in anterior shear, while fractures through the pedicles were most common for the destructive flexion tests. The data reported may be used to validate and inform computational models of cervical trauma, and could assist with developing cervical injury tolerances for ATDs with instrumented posterior elements.

ACKNOWLEDGEMENTS

The authors thank the Data, Design and Statistics Service, The University of Adelaide, for their assistance. Funding was provided by AOSpine Australia New Zealand (AOSAUNZ2015-03), the Royal Adelaide Hospital Research Fund, and the Australian Government's Research Training Program. C Jones is supported by a National Health and Medical Research Council (Australia) Early Career Fellowship.

CONFLICT OF INTEREST STATEMENT

No competing financial interests exist.

REFERENCES

Allen, B.L., Jr., Ferguson, R.L., Lehmann, T.R., O'Brien, R.P., 1982. A mechanistic classification of closed, indirect fractures and dislocations of the lower cervical spine. Spine (Phila Pa 1976) 7, 1-27.

Cholewicki, J., Panjabi, M.M., Nibu, K., Macias, M.E., 1997. Spinal ligament transducer based on a hall effect sensor. J Biomech 30, 291-293.

Cusick, J.F., Yoganandan, N., 2002. Biomechanics of the cervical spine 4: major injuries. Clinical Biomechanics 17, 1-20.

Cyron, B.M., Hutton, W.C., 1978. The fatigue strength of the lumbar neural arch in spondylolysis. The Journal of Bone and Joint Surgery 60-B, 234-238.

Cyron, B.M., Hutton, W.C., Troup, J.D., 1976. Spondylolytic fractures. The Journal of Bone and Joint Surgery 58-B, 462-466.

Foster, B.J., Kerrigan, J.R., Nightingale, R.W., Funk, J.R., Cormier, J.M., Bose, D., Sochor, M.R., Ridella, S.A., Ash, J.H., Crandall, J., Year Analysis of cervical spine injuries and mechanisms for CIREN rollover crashes. In 2012 International IRCOBI Conference on the Biomechanics of Injury. Dublin, Ireland.

Green, T.P., Allvey, J.C., Adams, M.A., 1994. Spondylolysis. Bending of the inferior articular processes of lumbar vertebrae during simulated spinal movements. Spine (Phila Pa 1976) 19, 2683-2691.

Hadley, M.N., Fitzpatrick, B.C., Sonntag, V.K., Browner, C.M., 1992. Facet fracture-dislocation injuries of the cervical spine. Neurosurgery 30, 661-666.

Hakim, N.S., King, A.I., Year Static and dynamic articular facet loads. In 20th Stapp Car Crash Conference. Dearborn, MI.

Hodgson, V., Thomas, L., 1980. Mechanisms of cervical spine injury during impact to the protected head. SAE Technical Paper 801300.

Huelke, D.F., Nusholtz, G.S., 1986. Cervical spine biomechanics: A review of the literature. Journal of Orthopaedic Research 4, 232-245.

Ivancic, P.C., 2012. Head-first impact with head protrusion causes noncontiguous injuries of the cadaveric cervical spine. Clin J Sport Med 22, 390-396.

Ivancic, P.C., Pearson, A.M., Tominaga, Y., Simpson, A.K., Yue, J.J., Panjabi, M.M., 2007. Mechanism of cervical spinal cord injury during bilateral facet dislocation. Spine (Phila Pa 1976) 32, 2467-2473.

Ivancic, P.C., Pearson, A.M., Tominaga, Y., Simpson, A.K., Yue, J.J., Panjabi, M.M., 2008. Biomechanics of cervical facet dislocation. Traffic Inj Prev 9, 606-611.

Jaumard, N.V., Welch, W.C., Winkelstein, B.A., 2011. Spinal facet joint biomechanics and mechanotransduction in normal, injury and degenerative conditions. Journal of Biomechanical Engineering 133, 071010.

King, A.I., Prasad, P., Ewing, C.L., 1975. Mechanism of spinal injury due to caudocephalad accleration. The Orthopedic Clinics of North America 6, 19-31.

Kumaresan, S., Yoganandan, N., Pintar, F.A., Maiman, D.J., Goel, V.K., 2001. Contribution of disc degeneration to osteophyte formation in the cervical spine: a biomechanical investigation. Journal of Orthopaedic Research 19, 977-984.

McElhaney, J., Snyder, R.G., States, J.D., Gabrielsen, M.A., 1979. Biomechanical Analysis of Swimming Pool Neck Injuries. SAE International.

Nightingale, R.W., McElhaney, J.H., Richardson, W.J., Myers, B.S., 1996. Dynamic responses of the head and cervical spine to axial impact loading. J Biomech 29, 307-318.

Nightingale, R.W., Sganga, J., Cutcliffe, H., Bass, C.R., 2016. Impact responses of the cervical spine: A computational study of the effects of muscle activity, torso constraint, and pre-flexion. J Biomech 49, 558-564.

Panjabi, M.M., Cholewicki, J., Nibu, K., Grauer, J., Vahldiek, M., 1998. Capsular ligament stretches during in vitro whiplash simulations. J Spinal Disord 11, 227-232.

Panjabi, M.M., Duranceau, J., Goel, V., Oxland, T., Takata, K., 1991. Cervical human vertebrae. Quantitative three-dimensional anatomy of the middle and lower regions. Spine (Phila Pa 1976) 16, 861-869.

Panjabi, M.M., Oxland, T., Takata, K., Goel, V., Duranceau, J., Krag, M., 1993. Articular facets of the human spine. Quantitative three-dimensional anatomy. Spine (Phila Pa 1976) 18, 1298-1310.

Panjabi, M.M., Simpson, A.K., Ivancic, P.C., Pearson, A.M., Tominaga, Y., Yue, J.J., 2007. Cervical facet joint kinematics during bilateral facet dislocation. European Spine Journal 16, 1680-1688.

Payer, M., Schmidt, M.H., 2005. Management of traumatic bilateral locked facets of the subaxial cervical spine. Contemporary Neurosurgery 27, 1-3.

Pollintine, P., Przybyla, A.S., Dolan, P., Adams, M.A., 2004. Neural arch load-bearing in old and degenerated spines. Journal of Biomechanics 37, 197-204.

Quarrington, R.D., Jones, C.F., Tcherveniakov, P., Clark, J.M., Sandler, S.J.I., Lee, Y.C., Torabiardakani, S., Costi, J.J., Freeman, B.J.C., 2017. Traumatic subaxial cervical facet subluxation and dislocation: epidemiology, radiographic analyses, and risk factors for spinal cord injury. The Spine Journal.

Robertson, D.G.E., 2004. Research methods in biomechanics. Human Kinetics, Champaign, IL.

Schindelin, J., Arganda-Carreras, I., Frise, E., Kaynig, V., Longair, M., Pietzsch, T., Preibisch, S., Rueden, C., Saalfeld, S., Schmid, B., Tinevez, J.-Y., White, D.J., Hartenstein, V., Eliceiri, K., Tomancak, P., Cardona, A., 2012. Fiji: an open-source platform for biological-image analysis. Nature Methods 9, 676-682.

Schulitz, K.P., Niethard, F.U., 1980. Strain on the interarticular stress distribution. Measurements regarding the development of spondylolysis. Archives of Orthopaedic and Trauma Surgery 96, 197-202.

Shah, J.S., Hampson, W.G., Jayson, M.I., 1978. The distribution of surface strain in the cadaveric lumbar spine. The Journal of Bone and Joint Surgery 60-B, 246-251.

Siegmund, G.P., Davis, M.B., Quinn, K.P., Hines, E., Myers, B.S., Ejima, S., Ono, K., Kamiji, K., Yasuki, T., Winkelstein, B.A., 2008. Head-turned postures increase the risk of cervical facet capsule injury during whiplash. Spine (Phila Pa 1976) 33, 1643-1649.

Siegmund, G.P., Myers, B.S., Davis, M.B., Bohnet, H.F., Winkelstein, B.A., 2001. Mechanical evidence of cervical facet capsule injury during whiplash: a cadaveric study using combined shear, compression, and extension loading. Spine (Phila Pa 1976) 26, 2095-2101.

Suezawa, Y., Jacob, H.A., Bernoski, F.P., 1980. The mechanical response of the neural arch of the lumbosacral vertebra and its clinical significance. International Orthopaedics 4, 205-209.

Vaccaro, A.R., Koerner, J.D., Radcliff, K.E., Oner, F.C., Reinhold, M., Schnake, K.J., Kandziora, F., Fehlings, M.G., Dvorak, M.F., Aarabi, B., Rajasekaran, S., Schroeder, G.D., Kepler, C.K., Vialle, L.R., 2016. AOSpine subaxial cervical spine injury classification system. European Spine Journal 25, 2173-2184.

Van Toen, C., Melnyk, A.D., Street, J., Oxland, T.R., Cripton, P.A., 2014. The effect of lateral eccentricity on failure loads, kinematics, and canal occlusions of the cervical spine in axial loading. Journal of Biomechanics 47, 1164-1172.

Wang, C.S., Chang, J.H., Chang, T.S., Chen, H.Y., Cheng, C.W., 2012. Loading effects of anterior cervical spine fusion on adjacent segments. Kaohsiung Journal of Medical Sciences 28, 586-594.

White, A.A., Panjabi, M.M., 1990. Clinical Biomechanics of the Spine. Lippincott.

Wu, G., Siegler, S., Allard, P., Kirtley, C., Leardini, A., Rosenbaum, D., Whittle, M., D'Lima, D.D., Cristofolini, L., Witte, H., Schmid, O., Stokes, I., 2002. ISB recommendation on definitions of joint coordinate system of various joints for the reporting of human joint motion--part I: ankle, hip, and spine. International Society of Biomechanics. Journal of Biomechanics 35, 543-548.

Figure 1: Specimen preparation: a) cervical functional spinal unit dissected of soft-tissue, with wood-screw and steel wire attached to the vertebral bodies. b) The specimen was positioned in a custom mold with the spinous processes pointing vertically, perpendicular to the base, such that the posterior surfaces of the vertebral bodies aligned with the top surface. The lateral anatomy was pressed into plasticine to hold the specimen in the desired orientation, and to prevent the facets being embedded. The mold was then filled with PMMA and a support bar was fixed to the posterior surfaces of the vertebral bodies. c) A lateral radiograph of the embedded specimen.

Figure 2: Lateral schematic of the mechanical testing setup used to apply the facet loading vectors thought to be experienced during supra-physiologic a) anterior shear (AS; red arrow), and b) flexion (blue arrow) motions. Loading was applied to the inferior facets of V2 via bilateral loading pins which simulated the opposing facets at the level of interest (superior facets of V3 in c). V1 is the superior vertebra adjacent to the level of injury and was included to provide a physiological boundary condition for the posterior elements of V2. Displacement of the loading pin was calculated from the Instron actuator linear variable differential transducer.

Figure 3: Specimens instrumented with tri-axial rosette strain gauges (left) and Optotrak marker-carriers (right).

Figure 4: An example filtered load-displacement plot for a destructive test in the flexion loading direction with the instant of initial failure indicated (red X). The load-displacement plot for the corresponding non-destructive test is also shown (inset). The red lines represent the linear region, from which the apparent facet stiffness was calculated.

Figure 5: Mean measured apparent facet stiffness for the anterior shear and flexion loading directions, grouped by the spinal level of the tested vertebra. p-Values for post-hoc analysis of the final multivariable linear mixed-effects model (α=0.05) are shown.

Figure 6: Mean measured a) maximum principal strain, b) maximum shear strain, and c) sagittal facet deflection measured at 47 N in the non-destructive tests. p-Values from the respective final multivariable linear mixed-effects models (α=0.05) are shown.

Figure 7: Mean measured a) failure load, b) sagittal facet deflection, c) maximum principal strain, and d) maximum shear strain at initial failure for simulated anterior shear and flexion loading. p-Values from the respective final multivariable linear mixed-effects models (α=0.05) are shown.

Figure 8: Fracture through the facet tip occurred for all specimens tested to failure in the anterior shear direction (left), while specimens failed under simulated flexion typically fractured through the pedicles (right).

Figure 9: Illustrations of the failure mechanisms observed for the anterior shear (a & b) and flexion (e & f) test directions, and the proposed equivalent in-vivo loading environments (c & d, and g & h, respectively). In both testing orientations, the initial point of contact was the geometric center of the articular surface, to replicate the center of pressure in the normal facet joint (blue dots; a, c, e & g). During testing in the simulated anterior shear direction the facets deflected away from the load vector (angle β, b) and the point of contact translated inferiorly towards the facet tip (red dots, b & d) until fracture occurred. In contrast, the contact location

remained constant for a majority of specimens tested to failure under simulated flexion, causing bending to occur about the pedicles (angle φ, f) through which fracture occurred for 6 specimens (f & h). AS = anterior shear.

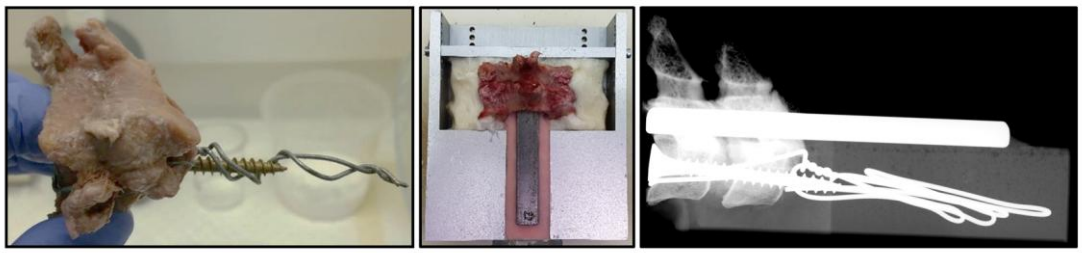

Figure 1 - suggest 1.5 column

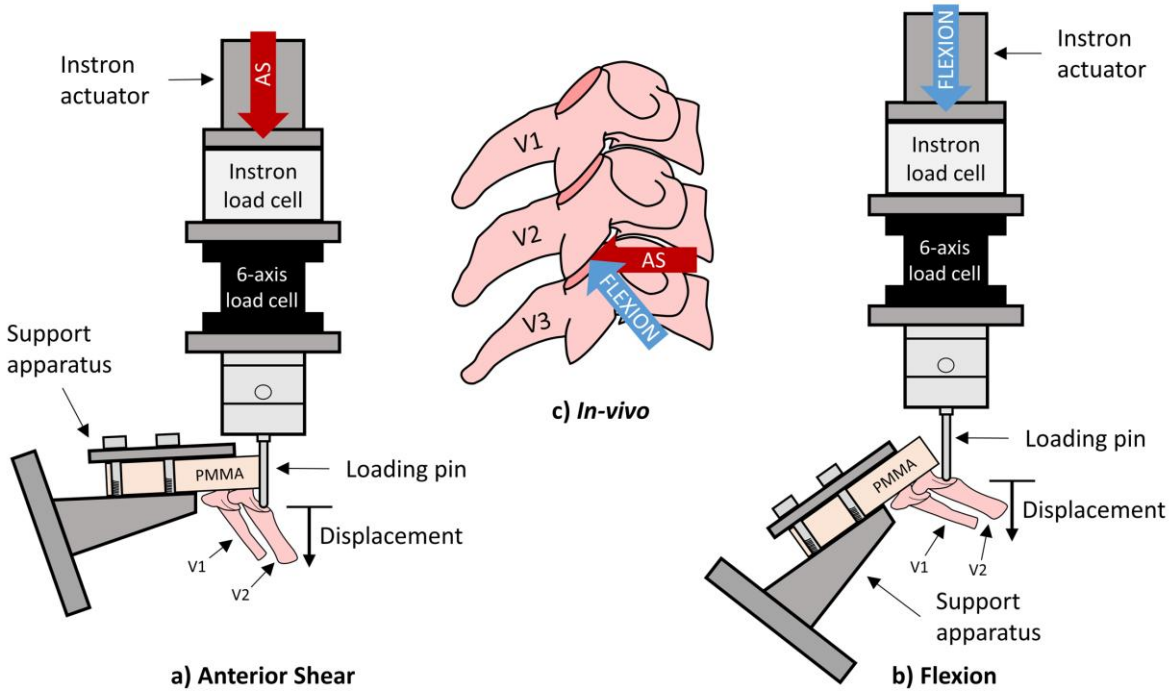

Figure 2 - suggest double column

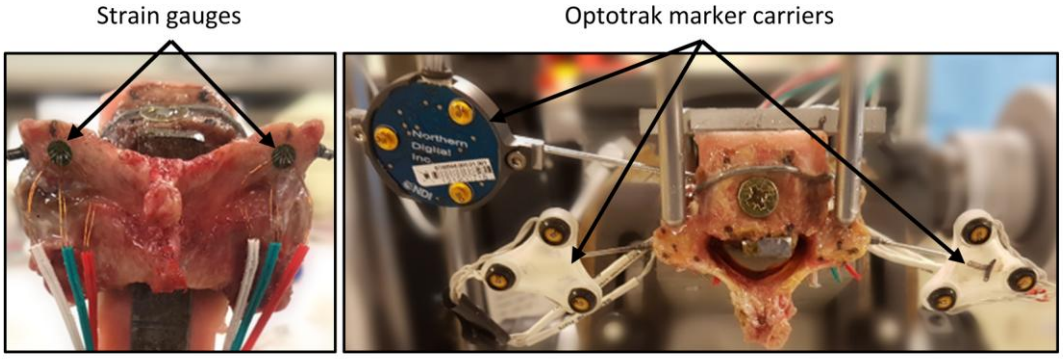

Figure 3 - suggest 1.5 column

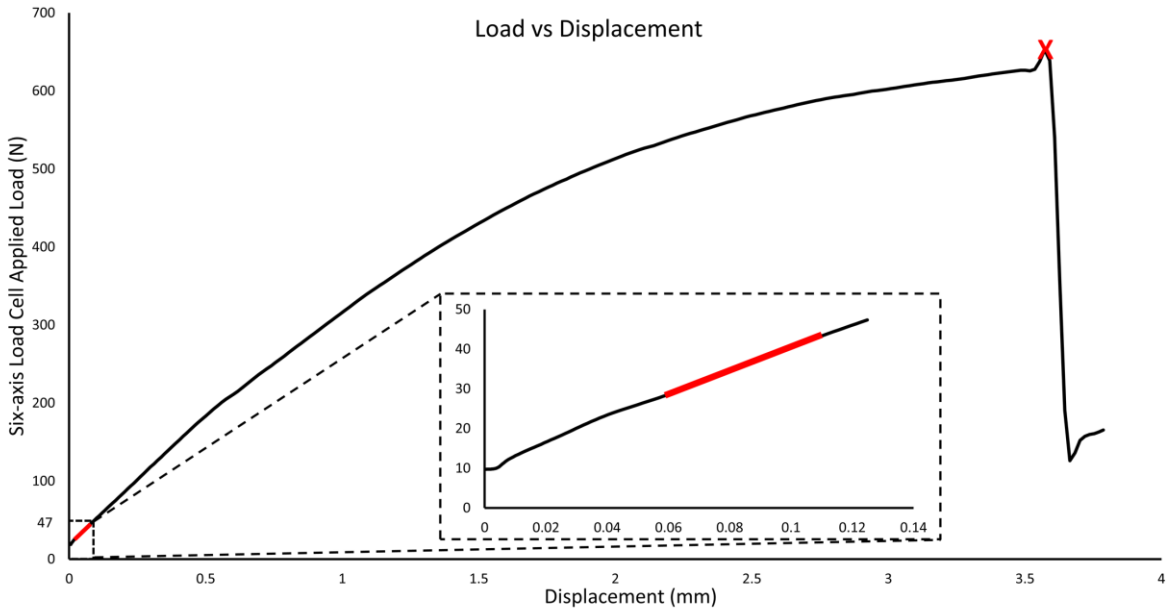

Figure 4 - suggest double column

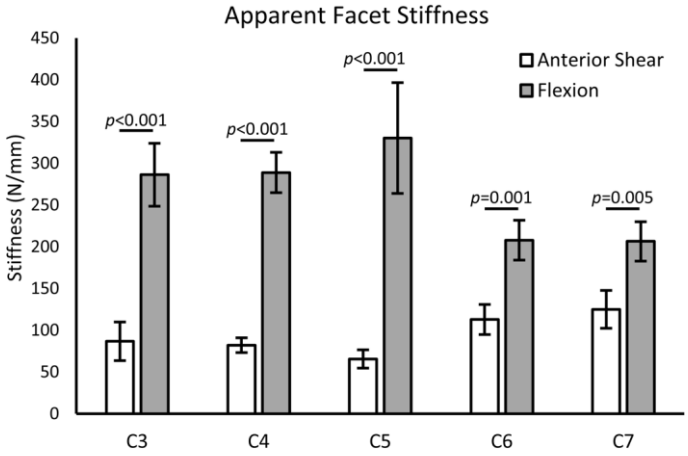

Figure 5 - suggest single column

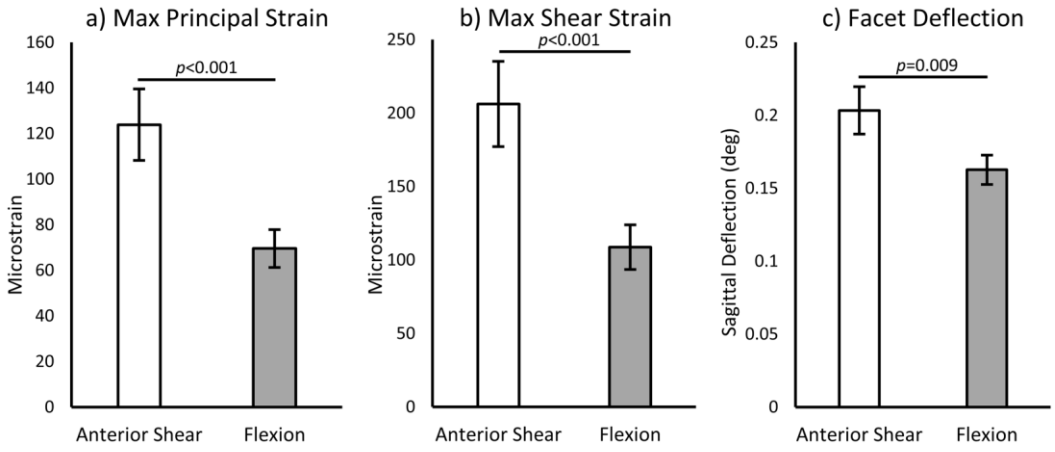

Figure 6 - suggest 1.5 column

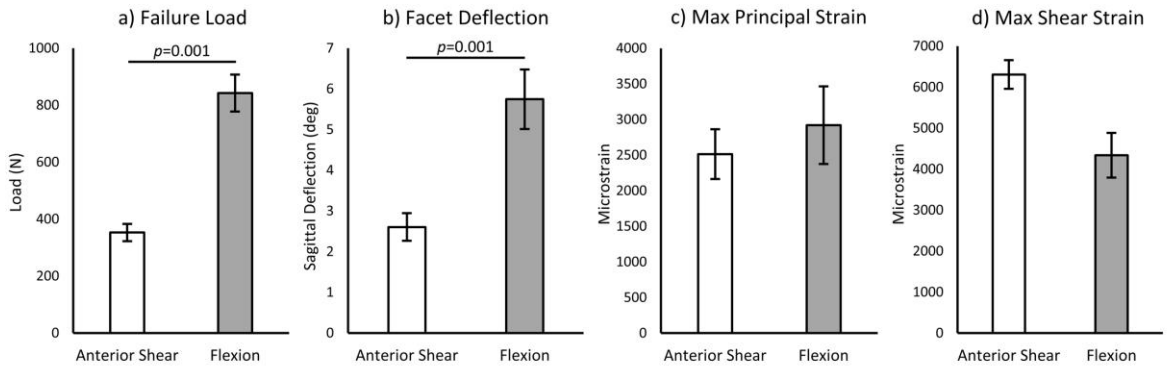

Figure 7 - suggest double column

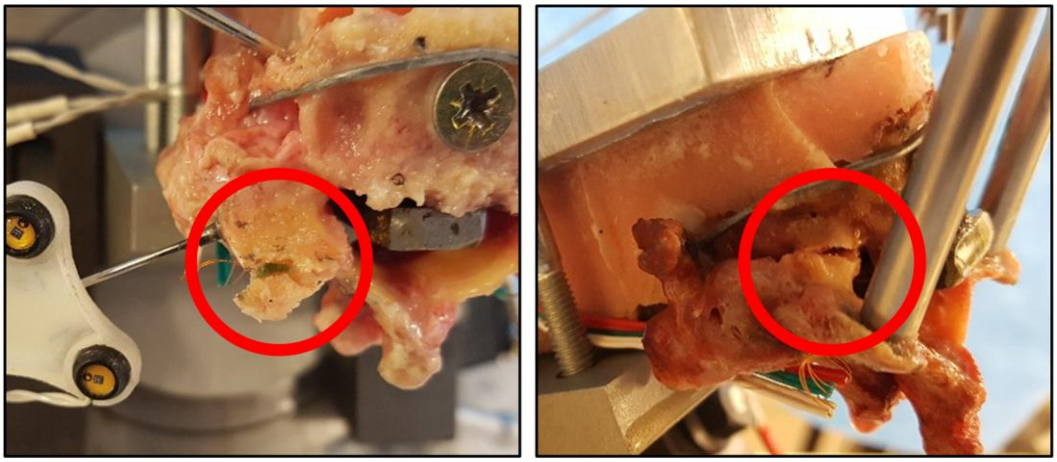

Figure 8 - suggest 1.5 column

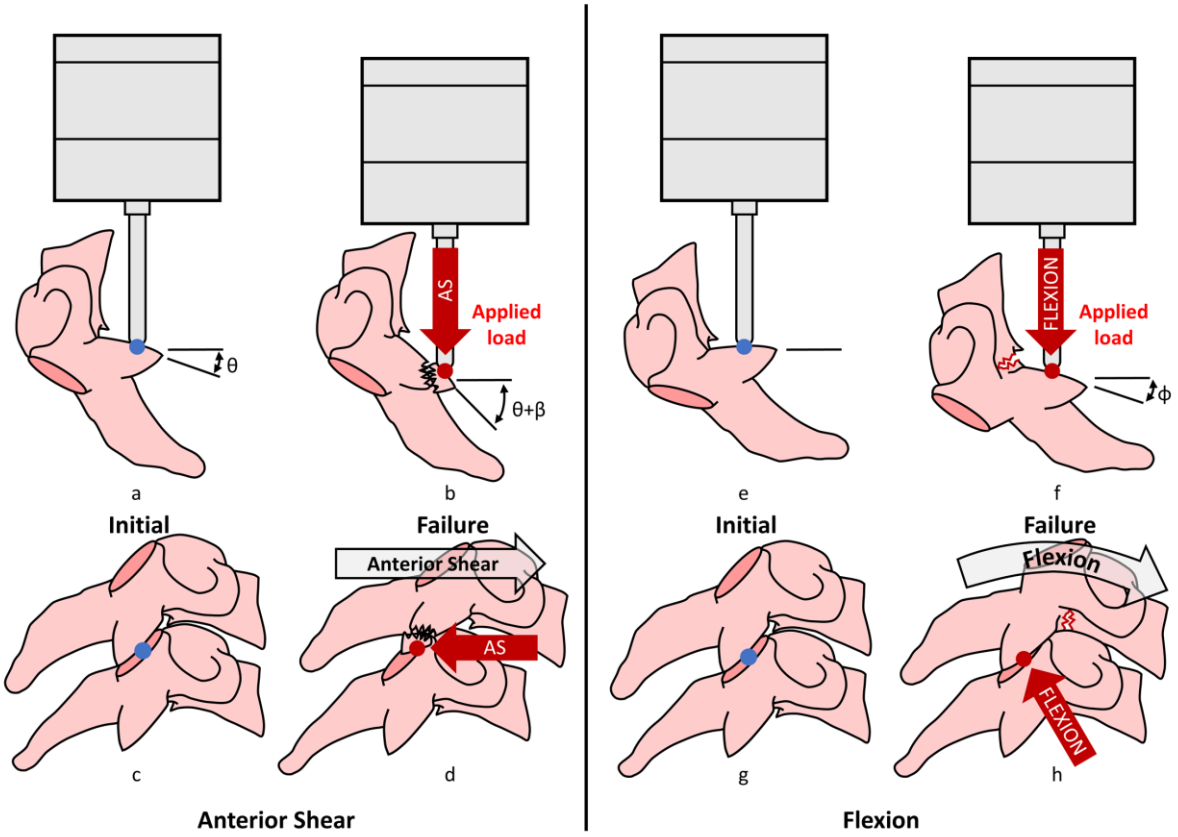

Figure 9 - suggest double column

Table 1: Donor and specimen details, and failure test outcome measures. vBMD = volumetric K2HPO4 equivalent bone mineral density (mg/cm^3). Dashes indicate that failure data was not available. Test 1 was omitted due to technical difficulties.

Test #	Specimen ID	Spinal Level	Sex	Age	Average vBMD	Failure Direction	Failure Load (N)	Failure Location
2	H023	C6	M	92	-27.3	-	-	-
3	H001	C3	M	48	192.2	Anterior Shear	226.4	Facet Tips
4	H001	C5	M	48	293.5	-	-	-
5	H001	C7	M	48	212.9	Anterior Shear	473.6	Facet Tips
6	H027	C4	F	64	177.7	Anterior Shear	336.3	Facet Tips
7	H012	C3	F	67	434.7	Flexion	822.7	Pedicles
8	H027	C6	F	64	142.2	Anterior Shear	330.8	Facet Tips
9	H012	C5	F	67	140.2	Anterior Shear	327.2	Facet Tips
10	H012	C7	F	67	118.5	Anterior Shear	292.3	Facet Tips
11	H017	C5	F	86	27.6	Anterior Shear	123.5	Facet Tips
12	H017	C3	F	86	34.3	-	-	-
13	H006	C4	M	57	238.5	-	-	-
14	H032	C7	M	65	161.0	Flexion	573.1	Facet Tips
15	H032	C3	M	65	161.0	Anterior Shear	316.4	Facet Tips
16	H006	C6	M	57	207.4	-	-	-
17	H032	C5	M	65	171.9	-	-	-
18	H045	C6	F	74	121.6	Anterior Shear	416.6	Facet Tips
19	H045	C4	F	74	136.6	Anterior Shear	405.9	Facet Tips
20	H039	C7	F	86	92.9	Flexion	873.5	Facet Bases
21	H039	C5	F	86	156.3	Flexion	1073.1	Facet Bases
22	H039	C3	F	86	194.2	Anterior Shear	382.5	Facet Tips
23	H018	C5	M	84	207.6	Flexion	1109.1	Pedicles
24	H018	C7	M	84	179.1	Anterior Shear	562.8	Facet Tips
25	H018	C3	M	84	209.2	Flexion	878.6	Pedicles
26	H026	C6	M	74	145.0	Anterior Shear	391.5	Facet Tips
27	H026	C4	M	74	140.4	Flexion	790.1	Pedicles
28	H021	C4	F	61	216.2	Flexion	658.4	Pedicles
29	H021	C6	F	61	179.6	Flexion	1203.4	Facet Bases
30	H044	C7	M	62	118.7	Flexion	743.8	Pedicles
31	H028	C6	M	50	127.2	Flexion	542.1	Facet Tips